JACS
JOURNAL OF THE AMERICAN CHEMICAL SOCIETY

COMMUNICATION

pubs.acs.org/JACS

Influence of Substrate Surface Chemistry on the Performance of Top-Gate Organic Thin-Film Transistors

Damien Boudinet,*[,†] Mohammed Benwadih,[†] Stéphane Altazin,[†] Jean-Marie Verilhac,[†] Eric De Vito,[†] Christophe Serbutoviez,[†] Gilles Horowitz,*[,‡] and Antonio Facchetti*[,§]

[†]CEA/LITEN/LCI, 17 rue des martyrs, 38054 Grenoble, France

[‡]ITODYS, CNRS UMR 7086 Université Paris Diderot, 15 rue Jean-Antoine de Baïf, 75205 Paris cedex 13, France

[§]Polyera Corporation, 8025 Lamon Avenue, Skokie, Illinois 60077, United States

Supporting Information

ABSTRACT: Organic thin-film transistor (OTFT) performance depends on the chemical characteristics of the interface between functional semiconductor/dielectric/conductor materials. Here we report for the first time that OTFT response in top-gate architectures strongly depends on the substrate chemical functionalization. Depending on the nature of the substrate surface, dramatic variations and opposite trends of the TFT threshold voltage (~±50 V) and OFF current ($10^5\times$!) are observed for both p- and n-channel semiconductors. However, the field-effect mobility varies only marginally (~2×). Our results demonstrate that the substrate is not a mere passive mechanical support.

Progress in organic thin-film transistors (OTFT) performance is the result of developing new organic semiconductors and dielectrics,[1] optimized active layer microstructure,[2] and enhanced understanding of charge trapping/injection/extraction at the device interfaces.[3] Thus, TFT mobilities of both p- and n-channel organic semiconductors are now similar to those of amorphous silicon-based devices, which is essential for pioneer applications.[4] OTFTs have been traditionally fabricated in the bottom-gate top-contact (BGTC) architecture on silicon (gate)/SiO_2 (dielectric) substrates.[5] In this configuration, self-assembled monolayers (SAMs) derived from silane organic reagents have been used to chemically modify the oxide dielectric surface and investigate semiconductor morphological and microstructural changes as well as charge trapping affecting TFT characteristics.[6] Indeed, several studies have reported large changes in carrier mobility (μ), threshold voltage (V_T), and other device parameters depending on the semiconductor type and the nature of the dielectric/SAM/semiconductor interface.[7] With the emergence of new solution-processable organic semiconductors, more studies focus on the top-gate bottom-contact (TGBC) architecture, considering the easier channel length scaling, reduced contact resistance, and self-encapsulation structure.[8] TGBC TFTs have been fabricated on plastic foils, but greater performances are generally observed with glass or silicon substrates.[9] A peculiarity of the TGBC architecture is that the semiconductor film is also in contact with the substrate. However, to our knowledge, no studies have systematically addressed chemical modifications of the substrate/semiconductor interface and whether this chemistry plays an important role in the TGBC device performance.

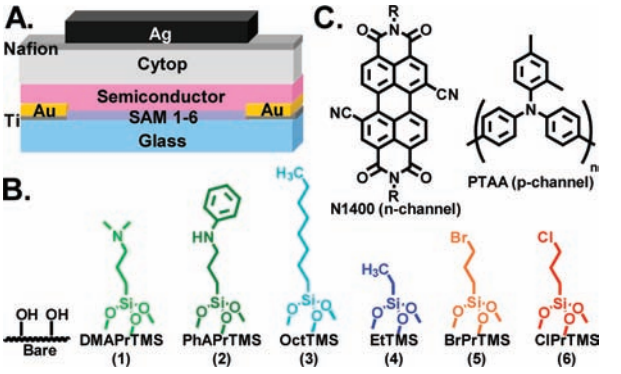

Figure 1. (A) Schematic representation of the TGBC TFT structure used in this study. Chemical structure of (B) the SAM precursors **1**−**6** and (C) the n-channel (N1400) and p-channel (PTAA) semiconductors.

In the work reported in this Communication, we fabricated TGBC TFTs where the glass substrate surface was functionalized with various SAMs prior to the deposition of the organic semiconductor (Figure 1A). Our results demonstrate that the electrical parameters of both n- and p-channel semiconductors strongly depend on the chemical characteristic of the SAM molecule, as in the case of conventional BGTC TFTs. Equally important, the electrical conductivity at $V_G = 0$ V, OFF current, and V_T variations versus SAM type exhibit opposite trends. Numerical simulations demonstrate that these effects originate from charge carrier density variations in the semiconductor film resulting from the combination of the SAM (E_{SAM}) and gate (E_G) electric fields.

TGBC TFTs (Figure 1A) were fabricated as described in the Supporting Information (SI). Briefly, glass slides having Ti/Au contacts (L = 100 μm, W = 1 cm) functionalized with various SAMs (Figure 1B) were used as substrates. The chemical functionalization of glass substrate surface was carried with trimethoxysilane precursors **1**−**6** following common procedures, and SAM formation is confirmed here by contact angle and XPS measurements (Table S1, Figures S1, S2). The SAMs used in this study

Received: February 2, 2011
Published: June 10, 2011

were selected to give a direct comparison with the abundant literature data available for SAM-functionalized BGTC TFTs.[7] The silane precursors were chosen because they contain alkyl/phenylamino (**1** and **2**), alkyl (**3** and **4**), and haloalkyl (**5** and **6**) functionalities, resulting in SAMs with tuned chemical structure, dipole moments/electric fields, and charge-transfer capabilities (Figure 1B). Indeed, several groups have shown that amino SAMs of type **1**/**2** favor electron accumulation, resulting in strong V_T shifts to positive values for both n-channel and p-channel BGTC TFTs versus electron-neutral alkyl (**3**/**4**) SAM-based TFTs, whereas halo SAMs of type **5**/**6** preferentially accumulate holes, leading to negative V_T shifts.[7] Two representative organic semiconductors were selected as channel materials: a core-cyanated perylene n-channel molecule (ActivInk N1400, Polyera Corp.) and a triarylamine p-channel polymer (PTAA) (Figure 1C). Prior to the semiconductor film deposition by spin-coating (~100 nm thick), 4-methoxythiophenol (for n-channel TFTs) and 4-fluorothiophenol (for p-channel TFTs) were grafted onto the gold to minimize the contact resistance.[10] The devices were completed by spin-coating a Cytop dielectric layer (~1.2 μm) and, to promote adhesion of the inkjet-printed Ag gate electrode, a thin Nafion layer (30 nm). All electrical measurements (Table 1) were performed at room temperature in the air (see SI).

To understand if the chemical modification of the substrate−semiconductor interface affects the semiconductor charge-transport characteristics, we first measured the source−drain current at different voltages while maintaining the gate in a floating configuration. Figure 2 shows that the $I-V$ plots for both semiconductors strongly depend on the SAM type. In the case of N1400 (n-channel, Figure 2A), halo-containing SAMs (BrPrTMS and ClPrTMS) lead to very low currents, whereas amino-functionalized surfaces (DMAPrTMS and PhAPrTMS) lead to a very high currents. The $I-V$ plots of the devices based on the electron-neutral substituents are midway between these two situations. Very interestingly, the opposite behavior is observed for PTAA TFTs (p-channel, Figure 2B).

The substantial current variations with the chemical functionalization of the substrate can be correlated with changes of the semiconductor film conductivity. This parameter was extracted from the slope of the $I-V$ characteristics at low bias (<|5| V); however, due to capacitive effects, these values are approximate. The results are given in Table 1. Clearly, both semiconductors exhibit large variations, depending of the SAM nature. The electrical conductivity is expressed by $\sigma = ne\mu_{bulk}$, where n is the charge carrier density, e is the elementary charge, and μ_{bulk} is the semiconductor bulk mobility. Since PTAA is an amorphous polymer and optical images, atomic force microscopy images, and X-ray diffraction plots of N1400 films are practically identical for all SAMs (Figures S3−S5), morphological/microstructural effects affecting bulk charge transport can be excluded. This is also supported by the opposite trends of the conductivity with the SAM type. Thus, the conductivity variations can only originate from charge carrier density changes within the semiconductor film, which is also evidenced by FET measurements (vide infra).

Next we investigated the TFT characteristics of these devices. Figure 2 shows the TGBC TFT transfer plots measured in the saturation regime (for output plots see Figures S6, S7). The saturation mobility and the threshold voltage were extracted using classical equations (Table 1). From these data it is clear that μ_{FET} of both types of semiconductor is minimally sensitive to the substrate chemical functionalization. Thus, the carrier mobility

Table 1. Electrical Parameters for TGBC TFTs based on substrates functionalized with Different SAMs[a]

SAM	σ [S/cm]	μ_{FET}[b] [cm^2/(V·s)]	V_T [V]	I_{ON}:I_{OFF}
N1400 (n-type) Semiconductor				
none[c,e]	–	$\sim 10^{-2}$	~+10	$\sim 10^3$
ClPrTMS	3.4×10^{-10}	1.4×10^{-2}	+47	1.0×10^5
BrPrTMS	2.9×10^{-9}	2.3×10^{-2}	+44	1.2×10^5
EtTMS	7.6×10^{-7}	2.3×10^{-2}	+32	7.3×10^4
OctTMS	8.8×10^{-7}	2.5×10^{-2}	+29	1.7×10^4
PhAPrTMS	3.7×10^{-6}	2.2×10^{-2}	+7	4.0×10^2
DMAPrTMS	1.1×10^{-5}	1.5×10^{-2}	+0	7.7×10^0
PTAA (p-type) Semiconductor				
none[d,e]	–	$\sim 3 \times 10^{-2}$	~−10	$\sim 10^3$
ClPrTMS	2.9×10^{-6}	4.8×10^{-3}	+16	6.5×10^1
BrPrTMS	6.5×10^{-6}	4.6×10^{-3}	+23	2.8×10^1
EtTMS	6.9×10^{-7}	5.9×10^{-3}	−3	2.7×10^2
OctTMS	2.4×10^{-7}	4.9×10^{-3}	+2	1.3×10^3
PhAPrTMS	4.6×10^{-9}	4.5×10^{-3}	−42	5.9×10^3
DMAPrTMS	2.4×10^{-10}	6.1×10^{-3}	−51	1.4×10^5

[a] Measured in ambient conditions. [b] Average of eight devices. [c] From ref 9a and this study. [d] From ref 12b. [e] Note that TFT performance on bare substrates, particularly V_T and I_{ON}:I_{OFF}, strongly depends on the glass quality and cleaning procedure.

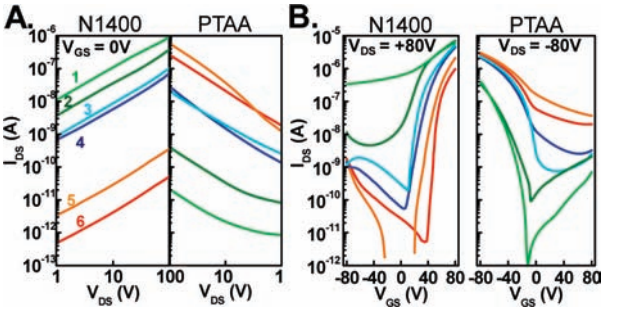

Figure 2. $I-V$ plots for TFTs with different SAMs measured (A) with a floating gate and (B) in the saturation regime at the indicated biases.

values of N1400 and PTAA are ~0.02 and ~0.005 cm^2/(V·s), respectively, similar to those found in previous investigations and on bare glass substrates.[9−12] This result is in agreement with the semiconductor film surface morphology which does not change with the SAM type (Figure S4) and the fact that the same gate dielectric is used in all of these devices. However, both V_T and I_{OFF}, and therefore the I_{ON}:I_{OFF} ratio and the V_{on}, strongly depend on the chemical functionalization of the substrate. Thus, for N1400-based TFTs, the V_T and I_{ON}:I_{OFF} (average) monotonically decrease: ~+45 V (SAM **1**/**2**) → ~+25 V (SAM **3**/**4**) → ~+4 V (SAM **5**/**6**) and ~10^5 (SAM **1**/**2**) → ~10^4 (SAM **3**/**4**) → ~10^1 (SAM **5**/**6**). Opposite trends are observed for the PTAA-based TFTs, with V_T and I_{ON}/I_{OFF} monotonically increasing (V_T more negative): ~+20 V (SAM **1**/**2**) → ~0 V (SAM **3**/**4**) → ~−47 V (SAM **5**/**6**) and ~10^1 (SAM **1**/**2**) → ~10^3 (SAM **3**/**4**) → ~ 1×10^5 (SAM **5**/**6**).

Similar silane-based SAMs were previously used to functionalize the dielectric surface of BGTC OTFTs, and significant V_T variations were reported.[7] For instance, Kobayashi[7a] and Pernstich[7b]

dx.doi.org/10.1021/ja2010576 | J. Am. Chem. Soc. 2011, 133, 9968–9971

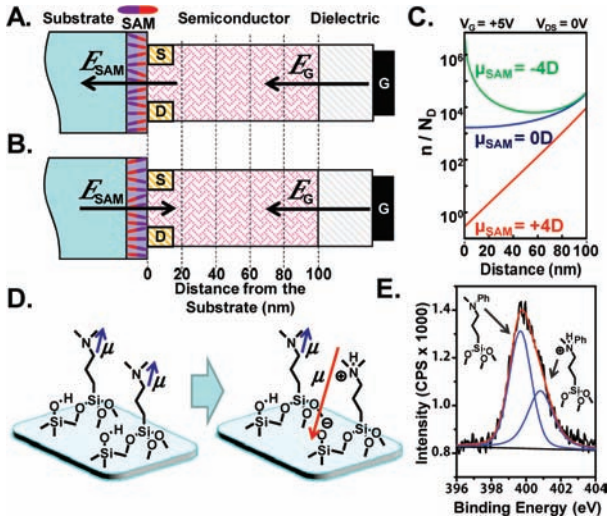

Figure 3. Schematics of the n-channel TFTs used in the simulation, having (A) negative and (B) positive SAM dipoles on the substrate surface. (C) Charge carrier density ratio as a function of the distance from the SAM−substrate surface with different dipole moments (semiconductor thickness = 100 nm). (D) Schematic representation of dipole inversion for SAM **1** (and **2**) due to partial proton transfer from the substrate surface −SiOH to the SAM amine group. (E) XPS spectra of SAM **2** on glass showing the presence of neutral (399.7 eV) and positively charged (400.8 eV) nitrogen types.

and co-workers showed that pentacene TFTs with the SiO_2 dielectric surface functionalized with alkylamino and perfluoroalkyl SAMs lead to charge accumulation and depletion, respectively (Figure S8). Opposite trends were found for fullerene TFTs. In either case, the charge carrier density variations versus alkyl SAM-based devices were attributed to dipolar effects of the SAM. Thus, the SAM functional group influences the molecular charge distribution, which in turn affects the surface potential in the semiconductor. This result was further supported by Kelvin probe[13] and conductivity[14] measurements as well as computations.[15]

To investigate whether the permanent polarization of a SAM grafted on the substrate surface can affect semiconductor charge distribution and compete with the field-effect carrier accumulation on the top channel, we carried out numerical simulations using the Comsol Multiphysics software (see SI).[16] To model the presence of the SAM and its dipole moment/field, two charged layers between the substrate and the semiconductor with opposite sign were used, as reported in the literature (Figures 3 and S9).[15] In this situation, the charge density of both layers can be directly linked to the molecular dipole moments of the SAM precursor, which were selected to vary from −4 D (Figure 3A) to +4 D (Figure 3B)—typical values for alkyl molecules with polar substituents.[13a,17] Solving Poisson's equation in the device, the charge carrier density in the semiconductor was computed as a function of the distance from the substrate surface. The results shown in Figure 3C were obtained for an n-channel semiconductor, and similar results are expected for p-channel TFTs (not shown).

From these simulations carried out for positive gate biases, it is clear that the substrate surface charge distribution derived from SAMs with negligible/small dipole moments ($\mu \approx 0$ D) will result, with most of the carriers (electrons for n-type TFTs) confined in the semiconductor films close to the dielectric interface (blue line). However, the electric field generated by dipolar SAMs ($\mu \neq 0$ D) grafted onto the substrate surface has profound effects on the overall semiconductor carrier density profile of these top-gate TFTs. Thus, substrates functionalized with SAM having a positive dipole moment (μ = +4 D here, red line) will result in a substantial depletion layer close to the interface with the substrate ($n < N_D$), substantially affecting the accumulated carrier on the opposite interface. The result is an overall reduction of the electron carrier density vs those based on electron-neutral SAMs, in agreement with the low OFF currents found experimentally for SAMs **5** and **6** and their computed dipole moment strengths and direction.[17,18] In contrast, TFTs with SAMs having a negative dipole moment (μ = −4 D, green line) should increase the overall electron density in the semiconductor, increase the OFF current, and decrease the I_{on}:I_{off} ratio. This is observed experimentally for the devices based on SAMs **1** and **2**; however, it disagrees with the computed/experimental molecular dipoles for these alkyl/arylamines or similar systems.[7a,17,19,20]

From these results, three important conclusions can be drawn: (1) Chemical functionalization of the substrate surface of top-gate TFTs is as important as the modification of the dielectric−semiconductor interface of other TFT architectures. (2) Because E_{SAM} and E_G do not overlap, the additional carriers induced by E_{SAM} cannot be depleted by the gate field. Thus, in contrast to bottom-gate TFTs, these TGBC devices can be considered all-ON TFTs, at least for the semiconductor thickness and E_G's investigated here. (3) The trends observed for TFTs based on SAMs **1** and **2** are the result of a permanent polarization of the amino SAMs, which *must be independent* of the semiconductor type. Several studies have explained electron accumulation/V_T shift of BGTC TFTs for amino-functionalized oxide surfaces via a charge-transfer mechanism due to the nitrogen lone pair.[7a] We believe that this phenomenon cannot explain the observed experimental/computational trends, since the same permanent polarization accounts for the V_T shifts for both n- and p-channel semiconductors. Because the LUMO energies of p-channel semiconductors are far higher than those of n-channel semiconductors, electron transfer from SAMs **1**/**2** to the semiconductor film cannot occur with the same extent and efficiency for both types of channel materials. Rather, we believe that protonation of some amino groups from the highly residual acidic silanol groups on the glass surface (Figure 3D) results in the formation of zwitterionic species, which inverts the molecular dipole vs the computed values and creates a permanent, semiconductor-independent SAM polarization. These data are clearly supported by the XPS measurements in Figure 3E for SAM **2**, which indicate the presence of substantial (~40%) positively charged SAM molecules.[21] Since amino SAM precursors are methoxy- and not chlorosilanes (thus MeOH and not HCl is the reaction byproduct), the only source of protonation must be the substrate, which is conceivable considering the comparable pK_a values of alkyl/arylammonium and silanols and well-documented interactions between silica surface and amines.[22]

■ ASSOCIATED CONTENT

Supporting Information. Contact angle and XPS measurements, OTFT fabrication details, numerical simulations, and complete ref 8. This material is available free of charge via the Internet at http://pubs.acs.org.

AUTHOR INFORMATION

Corresponding Authors
afacchetti@polyera.com; dboudinet@polyera.com; horowitz@univ-paris-diderot.fr

ACKNOWLEDGMENT

We thank D. Vuillaume for dipole moment computations and Mr. Kim for some XPS measurements.

REFERENCES

(1) (a) Arias, A. C.; MacKenzie, J. D.; McCulloch, I.; Rivnay, J.; Salleo, A. *Chem. Rev.* **2010**, *110*, 3. (b) Facchetti, A. *Chem. Mater.* **2011**, *23*, 733.

(2) (a) Lee, S. S.; Loo, Y.-L. *Annu. Rev. Chem. Biomol. Eng.* **2010**, *1*, 59. (b) Salleo, A.; Kline, R. J.; DeLongchamp, D. M.; Chabinyc, M. L. *Adv. Mater.* **2010**, *22*, 3812.

(3) (a) Chang, H.-C.; Ruden, P. P.; Liang, Y.; Frisbie, C. D. *J. Appl. Phys.* **2010**, *107*, 104502. (b) Kalb, W. L.; Haas, S.; Krellner, C.; Mathis, T.; Batlogg, B. *Phys. Rev. B* **2010**, *81*, 155315.

(4) (a) Zaumseil, J.; Sirringhaus, H. *Chem. Rev.* **2007**, *107*, 1296. (b) Klauk, H. *Chem. Soc. Rev.* **2010**, *39*, 2643.

(5) (a) Horowitz, G. *Adv. Mater.* **1998**, *10*, 365. (b) Capelli, R.; Toffanin, S.; Generali, G.; Usta, H.; Facchetti, A.; Muccini, M. *Nat. Mater.* **2010**, *9*, 496. (c) Piliego, C.; Jarzab, D.; Gigli, G.; Chen, Z.; Facchetti, A.; Loi, M. A. *Adv. Mater.* **2009**, *21*, 1573.

(6) (a) Kim, D. H.; Park, Y. D.; Jang, Y.; Yang, H.; Kim, Y. H.; Han, J. I.; Moon, D. G.; Park, S.; Chang, T.; Chang, C.; Joo, M.; Ryu, C. Y.; Cho, K. *Adv. Funct. Mater.* **2005**, *15*, 77. (b) Xie, H.; Alves, H.; Morpurgo, A. F. *Phys. Rev. B* **2009**, *80*, 245305. (c) Sirringhaus, H. *Adv. Mater.* **2009**, *21*, 3859. (d) Zschieschang, U.; Ante, F.; Schloerholz, M.; Schmidt, M.; Kern, K.; Klauk, H. *Adv. Mater.* **2010**, *22*, 4489.

(7) (a) Kobayashi, S.; Nishikawa, T.; Takenobu, T.; Mori, S.; Shimoda, T.; Mitani, T.; Shimotani, H.; Yoshimoto, N.; Ogawa, S.; Iwasa, Y. *Nat. Mater.* **2004**, *3*, 317. (b) Pernstich, K. P.; Haas, S.; Oberhoff, D.; Goldmann, C.; Gundlach, D. J.; Batlogg, B.; Rashid, A. N.; Schitter, G. J. *J. Appl. Phys.* **2004**, *96*, 6431.

(8) Gelinck, G. H.; et al. *Nat. Mater.* **2004**, *3*, 106.

(9) (a) Yan, H.; Zheng, Y.; Blache, R.; Newman, C.; Lu, S. F.; Woerle, J.; Facchetti, A. *Adv. Mater.* **2008**, *20*, 3393. (b) Boudinet, D.; Le Blevennec, G.; Serbutoviez, C.; Verilhac, J.-M.; Yan, H.; Horowitz, G. *J. Appl. Phys.* **2009**, *105*, 084510. (c) Verilhac, J. M.; Benwadih, M.; Altazin, S.; Jacob, S.; Gwoziecki, R.; Coppard, R.; Serbutoviez, C. *Appl. Phys. Lett.* **2009**, *94*, 143301.

(10) Boudinet, D.; Benwadih, M.; Qi, Y.; Altazin, S.; Verilhac, J.-M.; Kroger, M.; Serbutoviez, C.; Gwoziecki, R.; Coppard, R.; Le Blevennec, G.; Kahn, A.; Horowitz, G. *Org. Electron.* **2010**, *11*, 291.

(11) Ng, T. N.; Sambandan, S.; Lujan, R.; Arias, A. C.; Newman, C. R.; Yan, H.; Facchetti, A. *Appl. Phys. Lett.* **2009**, *94*, 233307.

(12) (a) Veres, J.; Ogier, S.; Loyd, G.; De Leeuw, D. M. *Chem. Mater.* **2004**, *16*, 4543. (b) Veres, J.; Ogier, S. D.; Leeming, S. W.; Cupertino, D. C.; Khaffaf, S. M. *Adv. Funct. Mater.* **2003**, *13*, 199.

(13) (a) Sugirama, H.; Hayashi, K.; Saito, N.; Nakagiri, N.; Takai, O. *Appl. Surf. Sci.* **2002**, *188*, 403. (b) Ofir, Y.; Zenou, N.; Goykham, I.; Yitzchaik, S. *J. Phys. Chem. B* **2006**, *110*, 8002.

(14) Calhoun, M. F.; Sanchez, J.; Olaya, D.; Gershenson, M. E.; Podzorov, V. *Nat. Mater.* **2008**, *7*, 84.

(15) Possaner, S. K.; Zojer, K.; Pacher, P.; Zojer, E.; Schürrer, F. *Adv. Funct. Mater.* **2009**, *19*, 958.

(16) Zimmerman, W. B. *Multiphysics Modelling with Finite Element Methods*; World Scientific: Singapore, 2006.

(17) Applequist, J.; Felder, C. E. *J. Chem. Phys.* **1981**, *75*, 1863.

(18) (a) Lewis, G. L.; Oesper, P. F.; Smyth, C. P. *J. Am. Chem. Soc.* **1940**, *62*, 3243. (b) Pacey, P. D.; Tan, Q.-T. N. *J. Phys. Chem.* **1995**, *99*, 17729.

(19) Profeta, S. J.; Allinger, N. L. *J. Am. Chem. Soc.* **1985**, *107*, 1907.

(20) Using MOPAC, we found the following dipole moments for **1**−**6** precursors: μSAM = +4.28 (**1**), +1.82 (**2**), 2.05 (**3**), +1.32 (**4**), +3.13 (**5**), and +3.34 D (**6**). Note that these values may differ from those of the molecules grafted on the substrate.

(21) (a) Dietrich, P. M.; Graf, N.; Gross, T.; Lippitz, A.; Krakert, S.; Schuepbach, B.; Terfort, A.; Unger, W. E. S. *Surf. Interface Anal.* **2010**, *42*, 1184. (b) Neoh, K. G.; Kang, E. T.; Tan, K. L *Polymer* **1993**, *34*, 1630.

(22) (a) Leung, K.; Nielsen, I. M. B.; Criscenti, L. J. *J. Am. Chem. Soc.* **2009**, *131*, 18358. (b) Child, M.; Heywood, M. J.; Yong, G. H.; Rochester, C. H. *J. Chem. Soc., Faraday Trans. 1* **1982**, *78*, 2005. (c) Liu, D.; Ma, G.; Allen, H. C. *Environ. Sci. Technol.* **2005**, *39*, 2025.